Received: 7 September 2024 | Revised: 30 December 2024 | Accepted: 20 January 2025

DOI: 10.1002/aic.18744

AIChE JOURNAL

RESEARCH ARTICLE

Transport Phenomena and Fluid Mechanics

On-aim generation of monodisperse droplets from piezoelectric pulsation-driven glass nozzles

Jinping Zha | Hong Zhu | Liangchao Shang | Yongchen Lu | Winston Duo Wu | Xiao Dong Chen | Jie Xiao

Particle Engineering Laboratory (China Petroleum and Chemical Industry Federation), School of Chemical and Environmental Engineering, College of Chemistry, Chemical Engineering and Materials Science, Soochow University, Suzhou, China

Correspondence
Jie Xiao, Particle Engineering Laboratory (China Petroleum and Chemical Industry Federation), School of Chemical and Environmental Engineering, College of Chemistry, Chemical Engineering and Materials Science, Soochow University, Suzhou, 215123 China.
Email: jie.xiao@suda.edu.cn

Funding information
National Natural Science Foundation of China, Grant/Award Numbers: 21978184, 22278284

Abstract

Piezoelectric pulsation-driven glass nozzles are capable of generating monodisperse droplets through liquid jet breakup. Due to the lack of fundamental understanding of this process, how to ensure uniform droplet generation with a specified size for liquids with specific rheological properties remains unknown. In this work, the complete atomization process including phenomena in and outside of the nozzle has been described by a new multi-physics model, where the expensive in-nozzle simulation can be rigorously replaced by a semi-empirical relationship. This computationally efficient model allowed us to systematically and quantitatively explore the influence of different material and operating parameters on jet breakup. It was found unintuitively that the surface tension has negligible influence on droplet size and its distribution. The droplet size can be independent of the nozzle radius under the condition of a constant inflow rate. Moreover, a detailed guideline was established to achieve on-aim size control of the atomized droplets.

KEYWORDS
atomization, droplet size distribution, liquid jet breakup, monodisperse droplet, piezoelectric pulsation

1 | INTRODUCTION

Across the communities of science, technology and industry, droplets are needed and utilized almost everywhere, among which the monodisperse ones with a specified size are of particular interest and value. For instance, in inkjet printing, the use of small and uniform ink droplets can significantly enhance printing resolution.[1] In microfluidic systems where droplets serve as individual microreactors,[2] ensuring precise control over the droplet size and monodispersity is essential for rapid and efficient reactions.[3] Moreover, spherical and uniform drug particles can optimize drug release kinetics.[4] In the realm of inhalation drug delivery, achieving an ideal droplet diameter of 2–5 μm holds paramount importance for enhancing drug delivery efficiency, as particles within this size range will undergo rapid absorption after deposition in the alveoli.[5]

Jet breakup, a fundamental research focus in fluid mechanics, has garnered significant theoretical and experimental attention. Plateau and Rayleigh provided foundational explanations using experimental and theoretical approaches. The former[6] elucidated this phenomenon by considering surface energy, whereby the jet's surface energy seeks a minimum state. Once the cylindrical jet surface undergoes deformation, this deformation does not recover, leading to the formation of spherical droplets characterized by a reduced surface area. Rayleigh[7] introduced a perturbation term of linear superposition into the hydrodynamic governing equation of the jet and determined that the breakup behavior of the jet is dictated by the fastest growth rate. Their contribution to jet breakup is known as Rayleigh-Plateau instability.

Based on this understanding, various experimental methodologies have been investigated to achieve uniform droplet production. Different atomizers such as rotary wheel atomizers, pressure nozzle atomizers, and pneumatic nozzles (namely dual fluid atomizers), have been manufactured to produce droplets with different sizes and distributions. A greater energy density often leads to smaller

droplets with a narrow span.[8] For rotary wheel atomizers, for example, different structures such as disc atomizers were made with grooves to allow a more homogeneous spray.[9] In microfluidics, achieving monodisperse droplets often typically involves manipulation of shear forces[10] or interfacial tension,[11] which can be controlled by varying channel geometry,[12,13] multiphase flow rates,[14] and fluid properties.[2] Understanding electrohydrodynamic deformation of single and double emulsion droplets induced by the combined DC electric and shear flow fields will offer valuable insights into the generation of streams of monodispersed droplets.[15,16]

External perturbations, such as those induced by electric fields[17] or mechanical perturbations,[18] are alternative strategies for the design of monodisperse droplet generators. Ozen et al.[19] applied distinct electric fields to both sides of microchannels, leading to deflection of the liquid–liquid interface. By controlling the amplitude of the electric field and the flow rate, the droplet size and the formation rate can be well controlled. Liu et al.[20] reported a new optofluidic resonating phenomenon that achieved uniform droplet generation by applying optical pressure to a liquid jet. This method involves the application of periodically varying perturbations to the upstream position of the jet, thereby triggering Rayleigh-Plateau instability and facilitating uniform droplet formation.

Due to easy control and excellent repeatability, piezoelectric perturbation has garnered widespread adoption. Duan et al.[21] integrated piezoelectric perturbation with flow focusing to produce highly monodisperse aerosols. Using a piezoelectric nozzle, Vassallo et al.[22] conducted experimental investigations on jet breakup and revealed four breakup modes under disturbances of different amplitudes and frequencies. Wu et al. designed a piezoelectric ceramic nozzle for generating monodisperse droplets[23] and employed it in spray drying to produce high-quality microparticles.[24,25]

The numerical simulation methodology has received significant attention given the unavailability of detailed information on liquid flow within the nozzle through experimental means and the inherent challenges in measurement. The numerical approach is helpful for obtaining an in-depth understanding of jet phenomena. For instance, Mu et al.[26] utilized numerical simulations to control droplet monodispersity by applying external perturbations (waveform, frequency, and amplitude) to the focusing flow. Their study sheds light on various flow patterns and the impact of waveforms on jet breakup, thereby offering guidance for employing axisymmetric focused flow with perturbation to generate droplets on demand. Xiao et al.[27] designed a ring piezoelectric ceramic and developed a multiphysics coupling piezoelectric nozzle jet model. Under stable injection conditions, uniform droplets with a diameter of ~80 μm could be generated on demand. Different waveforms were designed to ensure droplet uniformity for both on-demand and continuous inkjet printing, consequently enhancing the resolution of the inkjet printhead.[28]

Although considerable research has been carried out on monodisperse droplets, there is limited information on quantitative conditions necessary for generating uniform droplets of specific sizes. In order to generate uniform droplets, current practice demands significant trial and error efforts. It is crucial to bridge the gap between theoretical insights into liquid jet breakup and experimental practice so as to attain a comprehensive understanding of the droplet formation mechanism that can lead to on-aim control of the atomization process.

In this work, the piezoelectric nozzle is taken as an example. A new computationally efficient multi-physics model was developed to simulate the complete atomization process, where the distribution patterns of droplets produced by jet breakup under various conditions were systematically explored. Furthermore, the formation conditions of monodispersed droplets were discussed to obtain droplets of specific sizes.

2 | MODELING AND ANALYSIS METHODS

2.1 | Model construction

The geometry constructed for investigating the atomization process is illustrated in Figure 1. The complete piezoelectric pulsation-driven glass nozzle is depicted in Figure 1A. The blue part represents the feed liquid, which flows into the glass tube (in gray, with outer diameter R_t (m)) at the inlet flow rate q_{in} (g/min) and flows out from the bottom of the nozzle into the air domain (white area in Figure 1A). The piezoelectric ceramic (in red) surrounds the glass tube and acts on the fluid by applying a sinusoidal disturbance of the voltage ($U = U_{peak}\cdot\sin(2\pi ft)$) to the glass tube. The jet flowing out of the nozzle outlet breaks under this disturbance. Several parameters are defined for the following analysis—the droplet size, characterized by the diameter in the r direction (D_r (μm)) and the diameter in the z direction (D_z (μm)), along with the spacing between neighboring droplets denoted as S_d (μm) and the length of the unbroken liquid jet L_j (μm) (see Figure 1A).

The complete atomization model consists of two parts: the in-nozzle model above the nozzle outlet and the out-nozzle model below the outlet. Figure 1B provides a detailed view of the out-nozzle model, a crucial geometry to investigate liquid jet breakup and subsequent droplet formation. The left part shows the complete geometry of the air domain with a height of H_a (m) and the small upper domain representing the feed liquid area with a radius of R_n (m) and a height of $R_n/100$ (m) (see the enlarged view), which constitutes a part of the nozzle to ensure the model solvability. The liquid enters the air domain upon exiting the nozzle outlet. Subjected to the pulsation of the applied disturbance, a wavy liquid jet forms and then breaks into droplets. Given the inherent cylindrical symmetry of the nozzle, the droplets and surrounding flow fields are aligned along the central axis without azimuthal variations. As a result, both the in-nozzle and out-nozzle multi-physics models were developed as 2D axisymmetric models. This approach not only accurately captures the physics of the system, but also significantly reduces computational cost compared to full 3D models.

The governing equations and detailed initial and boundary conditions for both in-nozzle and out-nozzle multi-physics models have been introduced in our recent paper.[29] Major equations are recapped in the Supplementary Materials S1 and S2 respectively.

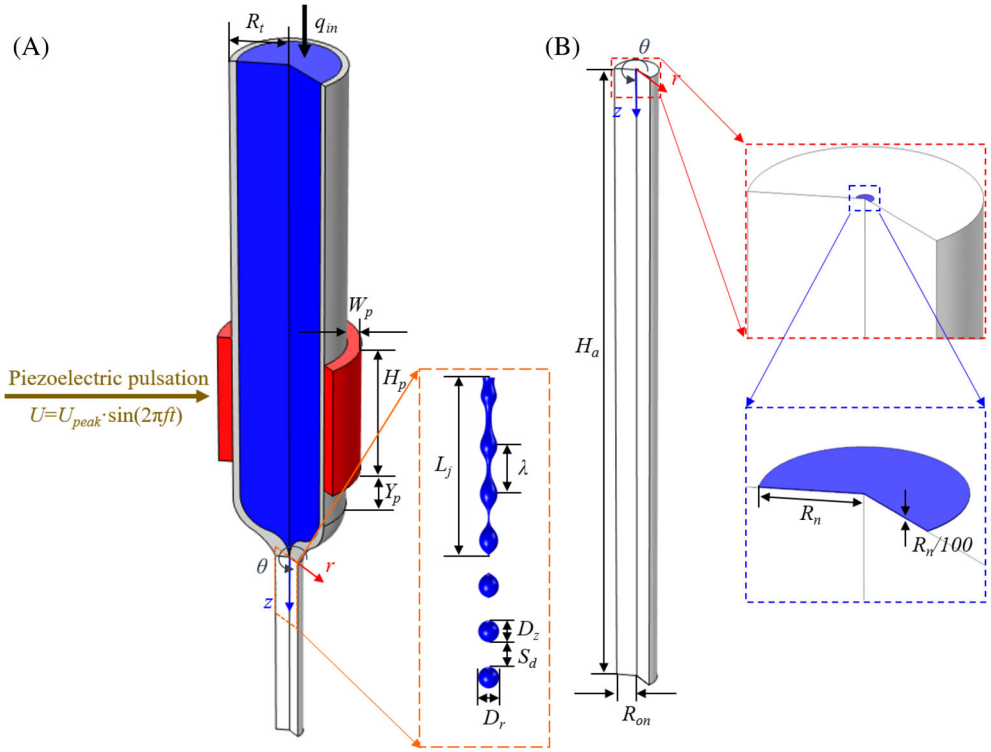

FIGURE 1 Model geometry and dimensions (3D view): (A) Complete geometry for the in-nozzle model and the out-nozzle model, and (B) details of the out-nozzle model. Liquid flows into the atomizer with an inflow rate q_{in}, and piezoelectric pulsation is applied to the piezoelectric ceramic (in red).

2.2 | Derivation of a semi-empirical relationship to replace in-nozzle multi-physics model

It is noteworthy that the nozzle deforms under the influence of the force applied by the piezoelectric ceramic. The relationship between the liquid volume and volume change can be expressed as follows:

$$V_{\text{volume}} = V_{0,\text{volume}} + \Delta V_{\text{volume}}, \tag{1}$$

where $V_{0,\text{volume}}$ (m^3) is the initial volume of the liquid in the nozzle chamber and ΔV_{volume} (m^3) is the volume change during the pulsation of the piezoelectric ceramic.

Because the potential applied to piezoelectric ceramics changes sinusoidally, the volume change ΔV_{volume} varies sinusoidally with time accordingly, that is,

$$\Delta V_{\text{volume}} = A_V \sin(2\pi ft), \tag{2}$$

where A_V (m^3) represents the maximum deformation of the volume.

The outflow rate should be a function of volume change:

$$q_{\text{out}} = q_{\text{in}} - \rho_l \frac{dV_{\text{volume}}}{dt}, \tag{3}$$

where ρ_l (kg/m^3) is the density of the liquid.

Combining Equations (1)–(3), the following relation can be obtained:

$$q_{\text{out}} = q_{\text{in}} - 2\pi\rho_l f A_V \cos(2\pi ft). \tag{4}$$

The average velocity at the nozzle outlet should be:

$$\bar{v} = \frac{q_{\text{out}}}{\rho_l \pi {R_n}^2}. \tag{5}$$

For a fully developed flow, the velocity distribution at the nozzle outlet should be given by:

$$v_{\text{outlet}} = 2\bar{v}\left(1 - \left(\frac{r}{R_n}\right)^2\right). \tag{6}$$

Combining Equations (4)–(6), the velocity at the nozzle outlet can be expressed as follows:

$$v_{\text{outlet}} = \frac{2}{\pi R_n^2}\left[\frac{q_{\text{in}}}{\rho_l} - 2\pi f A_V \cos(2\pi ft)\right]\left(1 - \left(\frac{r}{R_n}\right)^2\right) \tag{7}$$

serving as the inlet velocity of the out-nozzle model. This formulation expresses the outlet velocity of the in-nozzle model explicitly as a function of key operational and material property parameters. As a result, the complete atomization process can be simulated by solving only the out-nozzle model, using this function directly as the inlet boundary condition. This eliminates the need to solve the computationally expensive in-nozzle multi-physics model. The only unknown parameter, A_V, can be determined by fitting in silico experimental data from a set of pre-designed multi-physics in-nozzle simulations.

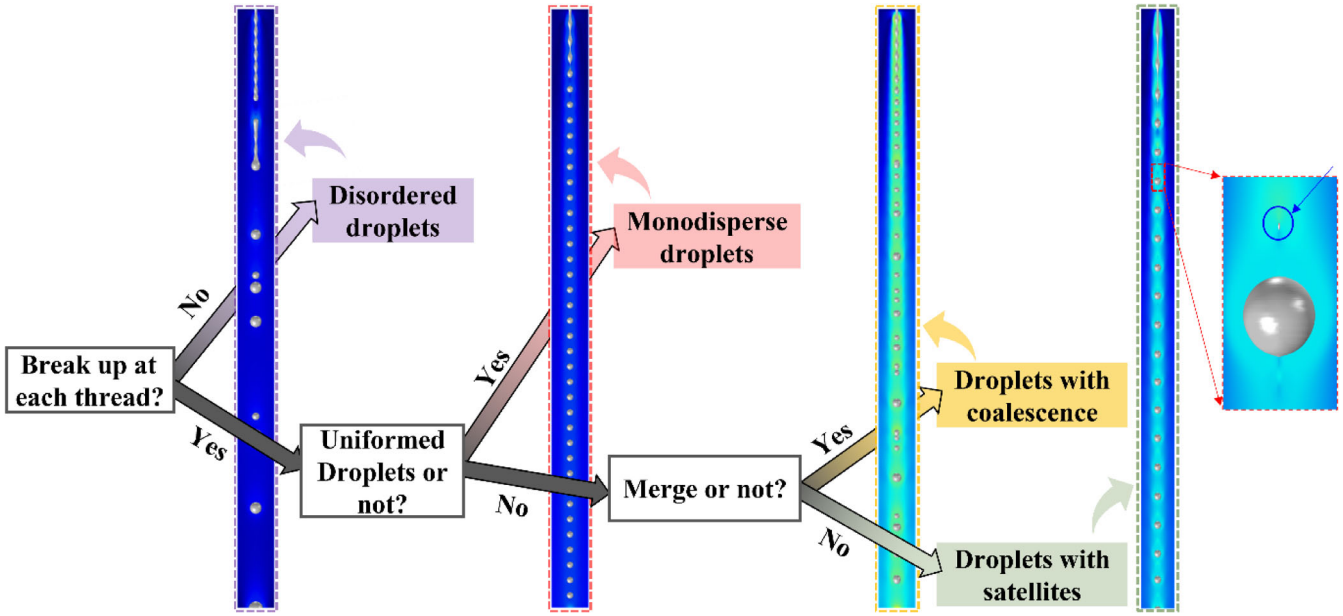

FIGURE 2 Four droplet distribution states together with the evaluation process.

2.3 | Analysis method

A dimensionless time is defined as

$$t^* = t \cdot f. \tag{8}$$

To characterize droplets of different sizes obtained in one in-silico experiment, the average diameter $\overline{D}$ and the dispersion index of droplets $\overline{D}^*$ are defined as follows:

$$\overline{D} = \frac{D_z + D_r}{2}, \tag{9}$$

$$\overline{D}^* = \frac{\overline{D}_{max} - \overline{D}_{min}}{\overline{D}_{min}} \times 100\%, \tag{10}$$

where $\overline{D}_{max}$, $\overline{D}_{min}$ are the maximum and minimum average diameters, respectively. Larger $\overline{D}^*$ indicates larger size range of droplets. When $\overline{D}^* = 0$, the droplets are exactly the same size. In this work, the droplets are considered to be monodisperse when $\overline{D}^* \leq 1\%$.

The droplets obtained under given conditions should belong to one of four distribution states: (1) disordered, (2) monodisperse/uniform, (3) with coalescence, and (4) with satellites. The breakup position, uniformity, and whether merging occurs can be used to distinguish the distribution states (see Figure 2 for details).

2.4 | System specifications

The liquid employed in the base case is the one adopted in the experimental study by Wu et al.[23] The parameters, including the piezoelectric ceramic parameters, nozzle parameters, and liquid properties are listed in Table 1 (marked in italics and bold). The droplet snapshots at 10 ms were adopted for distribution state identification, and 50 droplets were collected after 10 ms for size distribution analysis.

Structured meshes were used for all fluid dynamic regions in both models due to their high quality, while unstructured meshes were applied to the glass and piezoceramic regions. The in-nozzle model utilized 11,139 mesh elements, with a minimum grid size of 2.3 μm and a maximum size of 175 μm. In contrast, the out-nozzle model consisted of 117,929 mesh elements, with a minimum grid size of 4.375 μm and a maximum size of 7 μm. The time step was set to $T/40$ for the in-nozzle simulations and $T/2.5$ for the out-nozzle simulations. A time-step independence study is included in the Supplementary Material. Additionally, mesh independence studies and experimental validations were conducted to ensure the accuracy of the model. For further details, please refer to our recent paper[1] and the summarized contents provided in Supplementary Material S3.[29]

For the parametric study, the influences on atomization process from six parameters were considered (Table 1). When one of them was varied, the others remained the same as those in the base case. In order to identify the optimal conditions for uniform droplet generation, a total of 266 cases were designed to carry out parametric analyses. Twenty of them were selected for an in-depth parametric analysis of each factor (see Table 1).

3 | RESULTS AND DISCUSSION

3.1 | Determining the semi-empirical relationship to replace in-nozzle model

Since the voltage disturbance applied to the glass tube has the form $U = U_{peak} \cdot \sin(2\pi ft)$, the frequency and peak voltage are two key

TABLE 1 Parameter values used in the base case simulation and parametric study.

Parameters		Notation	Value
Operating and design parameters	Frequency	f (kHz)	4, ***8***, 12, 16
	Peak voltage	U_{peak} (V)	0, ***0.5***, 1, 1.5, 2
	Inflow rate	q_{in} (g/min)	1.0, ***1.3***, 1.6, 2.0
	Nozzle radius	R_n (μm)	25, 30, ***35***, 40
Liquid properties	Viscosity	μ (mPa·s)	35, ***54.4***, 75, 95
	Surface tension	σ (mN/m)	25, 45, ***65.61***, 85

Note: Base-case values are in italics and bold.

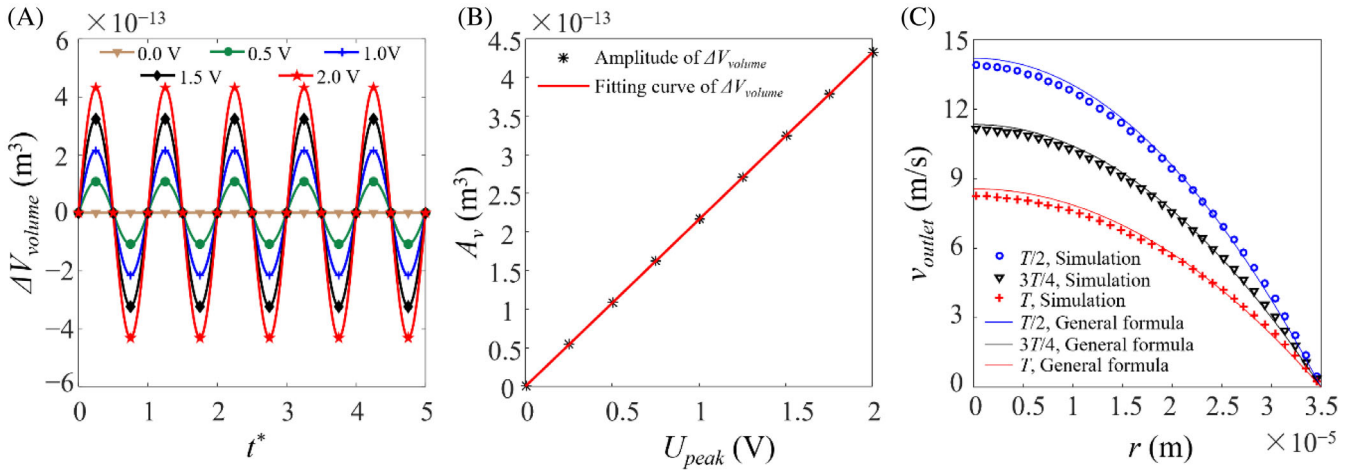

FIGURE 3 Results for deriving the semi-empirical relationship: (A) ΔV_{volume} changes with dimensionless time t^* under different voltages, (B) relationship between A_V and voltage, (C) comparison of outlet velocities predicted by the multi-physics in-nozzle simulation and calculated by the semi-empirical model.

operating parameters. The former controls the period of the cyclic disturbance while the latter governs the deformation depth of the glass tube. Furthermore, ΔV_{volume} is the key to determining the semi-empirical relationship by Equations (2) and (7). As shown in Figure 3A, it changes sinusoidally with time and increases with the voltage. To establish the relationship between ΔV_{volume} and the peak voltage, A_V (the amplitude of the ΔV_{volume}) was fitted against U_{peak} and a linear relationship was identified in Figure 3B. A constant coefficient k was introduced to represent the slope of this linear relationship, and Equation (7) can be written as follows:

$$v_{outlet} = \frac{2}{\pi R_n^2}\left[\frac{q_{in}}{\rho_l} - 2\pi f k U_{peak}\cos(2\pi f t)\right]\left(1-\left(\frac{r}{R_n}\right)^2\right). \quad (11)$$

Here, k was calculated to be 2.164×10^{-13} m^3/V. Different PZT geometries and their mount locations may lead to different values of k, which has been discussed in detail in the Supplementary Material S4.

Figure 3C shows a comparison between the calculated nozzle outlet velocity for the base case using the semi-empirical model (Equation (11)) and the simulated outlet velocity by the time-consuming multi-physics in-nozzle model. This semi-empirical relationship predicts quite well the multi-physics simulation data with a maximum difference of less than 5%. The parabolic profile of the outlet velocity also justifies the assumption of a fully developed flow at the outlet of the nozzle. The reliability of the semi-empirical relationship and the validity of the assumption of fully developed flow at the nozzle outlet are detailed in the Supplementary Material S5 and S6 respectively.

The multi-physics in-nozzle model involves several complex physical fields (electrostatics, solid mechanics, laminar flow and dynamic mesh), and the simulation of one case on a node of an HPC cluster (2 × Intel Xeon E5-2650v4 (2.2 GHz/12c)) cost about 2.1 h. However, to obtain the same velocity profile, the simple calculation based on the semi-empirical relationship (Equation (11)) will be instantaneous. As we have shown above, to obtain the unknown coefficient k for a specific piezoelectric nozzle, five in silico in-nozzle experiments under different voltages are sufficient. Subsequently, only the out-nozzle model needs to be solved to obtain information on the jet breakup and droplet distribution. With a semi-empirical relationship to replace the in-nozzle multi-physics model, this approach can save computational time significantly.

3.2 | Effects of different operating and design parameters on jet breakup

With the semi-empirical in-nozzle model, the effects of different parameters on jet breakup and droplet distribution can be obtained by numerically solving solely the multi-physics out-nozzle model.

This section explores the effects of operating and design parameters (i.e., frequency, peak voltage, inflow rate, and nozzle radius) on jet breakup. The corresponding results are presented in Figure 4.

The jet breakup and droplet distributions at 10 ms under different frequencies are shown in Figure 4A. At 1 kHz, the jet flows out of the nozzle and experiences perturbations due to the applied pulsation disturbance. Satellite droplets between two neighboring main droplets are produced due to the breakup of long and thin threads. At 4 kHz, the enhanced frequency shortens the distance between droplets, and steady perturbations result in monodisperse droplets with similar sizes and spacings (with dispersion index $\overline{D}^* = 0.37\%$, see Equation (10)). As the frequency increases to 8 kHz, more frequent perturbations result in smaller droplets and reduced spacings between them (with $\overline{D}^* = 0.07\%$). Monodispersed droplets produced under different frequencies are quantified in Figure 4E, both droplet sizes and spacings follow a decreasing trend with the increase of frequency. When the frequency is further increased to 12 kHz, this higher disturbance frequency destabilizes the jet, resulting in irregular breakup times and varying droplet spacings. Consequently, closely spaced droplets tend to merge to form larger droplets ($\overline{D}^* = 35.71\%$). At an even higher frequency of 16 kHz, the disturbance becomes too rapid to form effective jet perturbation, causing the jet to fall like a liquid column. Thick threads prevent the liquid jet from breaking up easily, leading to random break-ups. Randomly distributed droplets are produced with larger and irregular sizes, with $\overline{D}^*$ reaching 222.32%.

The jet breakup and droplet distributions at 10 ms under different peak voltages are illustrated in Figure 4B. When the voltage is zero (no applied pulsation), the liquid flows from the nozzle outlet as a continuous liquid column. When a voltage of 0.5 V is applied, the liquid jet oscillates and forms several wavy shapes, resulting in a decrease in the jet length and ultimately jet breakup into a series of droplets. Under regular oscillation, the droplets maintain a consistent shape and size (with $\overline{D}^* = 0.07\%$). Increasing the voltage to 1.0 V results in stronger perturbations, and the air velocity increases accordingly (see Figure 4B), leading to larger spacings between droplets. A higher voltage of 1.5 V causes the wavy jet to become quasi-spherical, resembling a "beads-on-a-string" configuration.[30] When the voltage reaches 2.0 V, long and thin threads between droplets break, ending up with individual and tiny satellite droplets (see magnified figure at 2.0 V in Figure 4B) that are unable to merge with the main droplets (with $\overline{D}^* = 699.95\%$). For the cases where monodispersed droplets can be produced, Figure 4F presents the corresponding quantified results. Notably, the droplet sizes remain almost constant, indicating that droplet size is almost independent on the voltage. While the spacing between neighboring droplets gets larger with an increasing voltage due to the increased nozzle outlet velocity.

The droplets exhibit varying distribution states under different inflow rates, and the corresponding results are shown in Figure 4C. According to Equation (11), liquid jet velocity at nozzle outlet gets larger with increased inflow rate. At 1.0 g/min, the liquid jet has a low velocity and does not break up at each thread between neighboring perturbations, resulting in irregularly sized droplets. Increasing the inflow rate to 1.3 g/min leads to a noticeable difference in size between the thickest and thinnest width of the liquid jet. The liquid jet appears shorter and breaks into droplets with regular sizes and spacings, exhibiting a monodisperse distribution with $\overline{D}^* = 0.07\%$. When the inflow rate is further increased to 1.6 g/min, a similar phenomenon to that at 1.3 g/min can be observed, with regularly distributed droplets but only with larger spacings and diameters due to the increased velocity ($\overline{D}^* = 0.09\%$). Furthermore, further increase of the inflow rate to 2.0 g/min increases both the droplet diameter and spacing. The thread between neighboring droplets forms a thin string, which breaks at both ends, forming tiny droplets. The longer threads, accompanied with higher velocities, also result in longer liquid jet lengths (see red dashed lines). It is interesting to observe that satellite droplet shows up at 10 ms for the case at 2.0 g/min (see the snapshot with the magnifying glass at 2.0 g/min in Figure 4C), while Figure 4G exhibits a monodisperse distribution with $\overline{D}^* = 0.05\%$ at 2.0 g/min. Furthermore, the case at 1.8 g/min between two monodispersed cases produces satellites with $\overline{D}^* = 731.26\%$. These unusual phenomena at 1.8 and 2.0 g/min imply that the produced unsteady satellite droplets may either merge with the main droplet or persist as isolated droplets. According to the quantified results of monodispersed droplets in Figure 4G, both droplet size and spacing between neighboring droplets are increased with increased inflow rate. Therefore, in addition to frequency, adjusting inflow rate is another effective way to manipulate the size of monodispersed droplets.

In Figure 4D, various jet breakup modes and droplet distribution states corresponding to different nozzle radii are depicted. Liquid jet velocity shows a decreasing trend with increasing nozzle radius, which aligns with the trend indicated by Equation (11). For a nozzle radius of 25 μm, a liquid jet exhibiting "beads-on-a-string" with very long, thin threads between droplets results in the production of satellite droplets (see the magnifying glass for the case of 25 μm in Figure 4(D)). With the nozzle radius increased to 30 μm, satellite droplets are formed during jet breakup. The monodisperse distribution with $\overline{D}^* = 0.35\%$ indicates that the satellite droplets eventually merge with the main droplets to form a series of monodisperse droplets. As the nozzle radius further increases to 35 μm, the droplets display similar shapes and sizes (monodisperse distribution with $\overline{D}^* = 0.07\%$), only with a decrease in the spacing between droplets due to the reduction in jet velocity caused by the increase in radius. As the nozzle radius goes up to 40 μm (see Figure 4D), the liquid jet remains similar to a liquid column. This occurs because the nozzle radius is too large, and the disturbance is incapable of breaking such a thick jet. Under weak disturbances, the liquid jet descends until the inertial force and gravity can no longer balance the surface tension force, resulting in jet instability and the formation of droplets of different sizes. Cases with nozzle radius between 30 and 35 μm that can produce monodispersed droplets are compared in Figure 4H. It indicates that spacings between neighboring droplets decrease with the increase of nozzle radius, which results from the decreasing jet velocity (see Figure 4D which shows the air velocity). The droplet size, however, is independent on the nozzle radius (see the red line in Figure 4H) under the condition of a constant inflow rate. This finding appears counterintuitive, since for experimentalists, adjusting the nozzle size is commonly

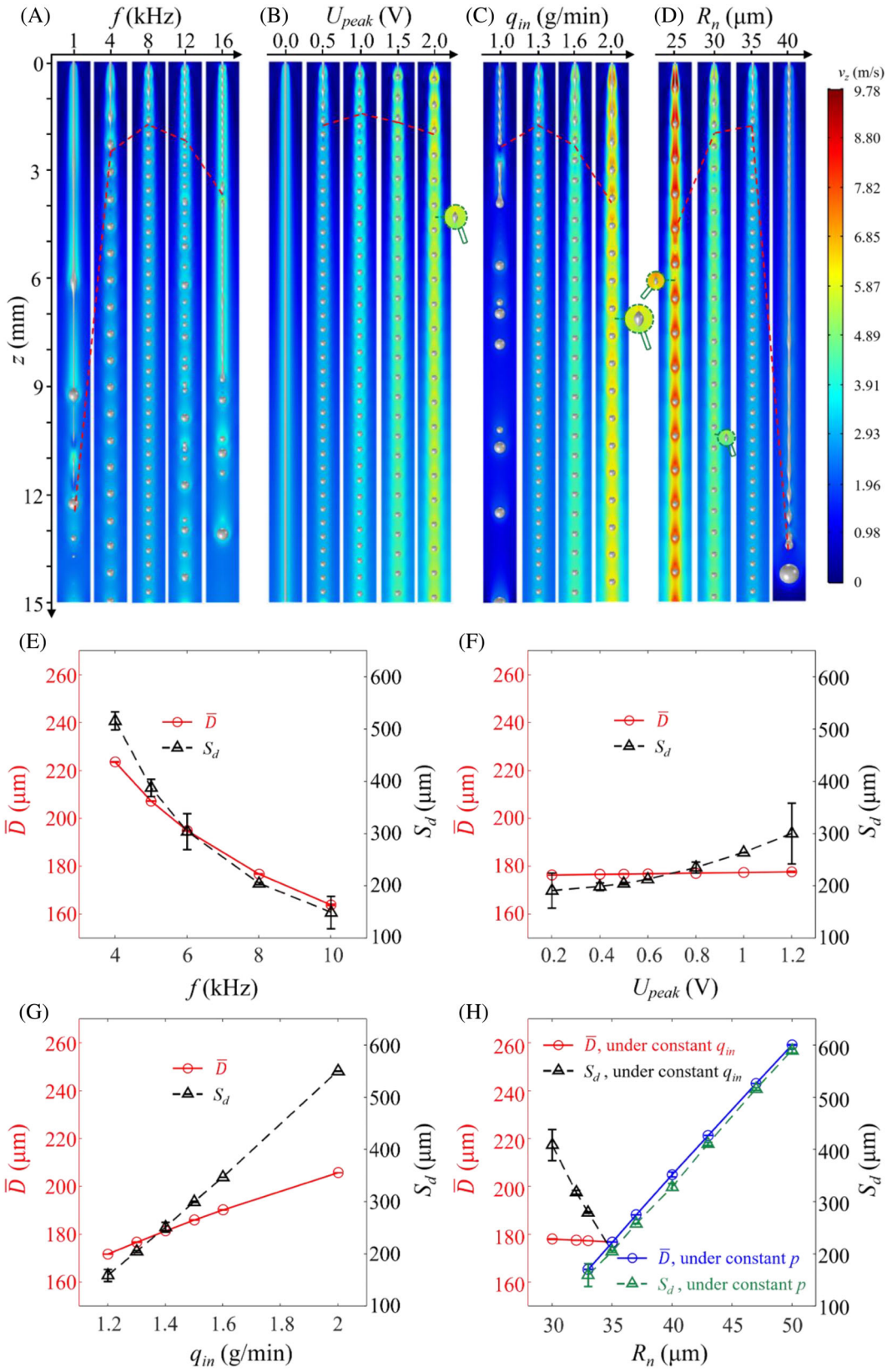

FIGURE 4 Results under different operating and design conditions, which include (A), (E) frequency, (B), (F) peak voltage, (C), (G) inflow rate, and (D), (H) nozzle radius. (A)–(D) display droplet distribution snapshots at 10 ms, with red dashed lines marking the jet breakup positions; (E)–(H) quantify distributions of the average diameter of 50 mono-disperse droplets and average spacing between them collected after 10 ms at the outlet of the out-nozzle model. Results are presented as mean ± SD. Magnifying glasses (having a powder of 10×) are used to magnify the satellite droplets, which are not visible in the original dimensions.

used to control the size of the droplets, with the droplet size estimated to be approximately twice the size of the nozzle.[31] In fact, if the inflow rate remains unchanged, altering the nozzle radius has no effect on the volume of liquid flowing from the nozzle outlet, thereby not affecting droplet size. In most experiments, the nozzle is operated at a constant pressure rather than a constant inflow rate.[32] To quantitatively understand two different operational modes, droplet distribution states with varying nozzle radii under constant pressure were also explored. As shown in Figure 4H, unlike the phenomenon observed under a constant inflow rate, under a constant pressure, the spacing between neighboring droplets increases with increasing nozzle radius. Consistent with experimental observations, droplet size increases almost linearly with nozzle radius under a constant pressure condition. Increasing nozzle radius under a constant pressure can lead to an increase of inflow rate. Increase of both radius and inflow rate contributes positively to the increase of droplet size. The droplet size is approximately 2.5 times the nozzle outlet size under the constant pressure condition. More theoretical efforts are needed in future to accurately predict the quantitative relationship between droplet size and nozzle radius.

Furthermore, by comparing the cases under different operating and design parameters (see Figure 4A–D), it is interesting to observe that the liquid jet length always shows a trend that initially decreases and then increases as the parameter value increases. This behavior is closely related to the liquid jet breakup mode, where both too small or too large parameter values result in nonuniform droplets. Considering all four parameters, the droplet distribution states follow a specific trend: disordered droplets, with coalescence, monodisperse droplets, and droplets with satellites. Two parameters play a crucial role in jet breakup and subsequent droplet formation: (1) disturbance frequency and (2) jet velocity. Higher frequencies and lower jet velocities are more likely to produce disordered droplets, while lower frequencies and larger air velocities are more likely to produce droplets with satellites. Regarding the droplet sizes of monodisperse droplets, disturbance frequency and inflow rate are two dominant factors that can influence droplet size. Note that adjusting nozzle radius under constant pressure can be treated as an alternative way to control inflow rate. Therefore, adjusting these two parameters accordingly can potentially realize the on-aim size control of atomized droplets. Section "Guidelines for on-aim-sized monodisperse droplet generation" in the following text will introduce the detailed procedure.

3.3 | Effects of different liquid properties on jet breakup

Rheological properties of liquids influence the atomization process as well. The droplet formation processes from liquids with different viscosity and surface tension values are illustrated in Figure 5. An increase in viscosity results in greater difficulty in breakup (see the red dashed lines showing the longer jet length under higher viscosity), decreasing jet velocity, and consequently varying jet breakup patterns. As shown in Figure 5A, when the viscosity is 35 mPa·s, the liquid jet under perturbations has thin threads that regularly break up to form monodisperse droplets with $\overline{D}^* = 0.001\%$. As the liquid viscosity increases to 54.4 mPa·s, the liquid jet thickens, and a lower jet velocity reduces the distance between neighboring droplets. The monodisperse distribution state is also identified in this case with $\overline{D}^* = 0.07\%$.

The quantified results of monodispersed droplets under different viscosities are shown in Figure 5(C). The spacings between neighboring droplets show a decreasing trend with the increase of viscosity, which can be attributed to the reduction of the jet velocity. For droplet size, although the trend seems not monotonic, the maximum and minimum sizes differ by no more than 2 μm. Therefore, viscosity is not considered as a significant factor that can influence the size of monodispersed droplets. Further increasing the viscosity to 75 mPa·s leads to an even thicker liquid jet. The disturbance on the liquid jet is unable to break two neighboring droplets at a similar jet length as in the case with lower viscosities, resulting in a longer liquid jet. The prolonged jet and unstable state at 75 mPa·s cause irregular droplet pinch-off, resulting in some neighboring droplets merging into larger droplets due to insufficient spacing. When the viscosity rises to 95 mPa·s, there is no significant difference in the size of the perturbation radius or the radius of the long liquid jet threads. The liquid jet may break up at any location, resulting in the formation of irregular droplets with $\overline{D}^* = 423.90\%$.

The results for different surface tensions are shown in Figure 5B. Surface tension, which is the force that minimizes droplet surface area. The liquid jet with larger surface tension is more likely to break to form droplets. Consequently, a higher surface tension leads to a shorter jet length (as indicated by the red dashed lines). Figure 5B also shows that the jet velocity exhibits a slight decreasing trend with the increase of surface tension, which reduces the spacing between neighboring droplets (see quantified results in Figure 5D). Furthermore, the droplet size shows a slight decreasing trend (almost negligible, less than 3 μm decrease for a 178.8 μm droplet) with the increase of surface tension (from 15 to 85 mN/m). No significant differences can be observed for the droplet distribution states, and nonuniform droplets are not produced under the investigated conditions. All cases exhibit mono-dispersity with $\overline{D}^* < 1\%$. Therefore, it can be concluded that surface tension mainly affects where the jet breaks (i.e., the jet length) and has a negligible effect on the jet breakup mode and droplet size. For the piezoelectric pulsation-driven glass nozzle operated under a constant inflow rate, tailoring either the fluid's viscosity or its surface tension cannot effectively control the droplet size.

3.4 | Guidelines for on-aim-sized monodisperse droplet generation

The above systematic analyses show how the droplet distribution state changes with the variations of the studied parameters, including operating conditions and design parameters for the piezoceramic nozzle (f, U_{peak}, q_{in}, and R_n) and liquid properties (μ and σ). To achieve monodisperse droplet generation, and hence on-aim size control of the atomized droplets, it is important to obtain a comprehensive and

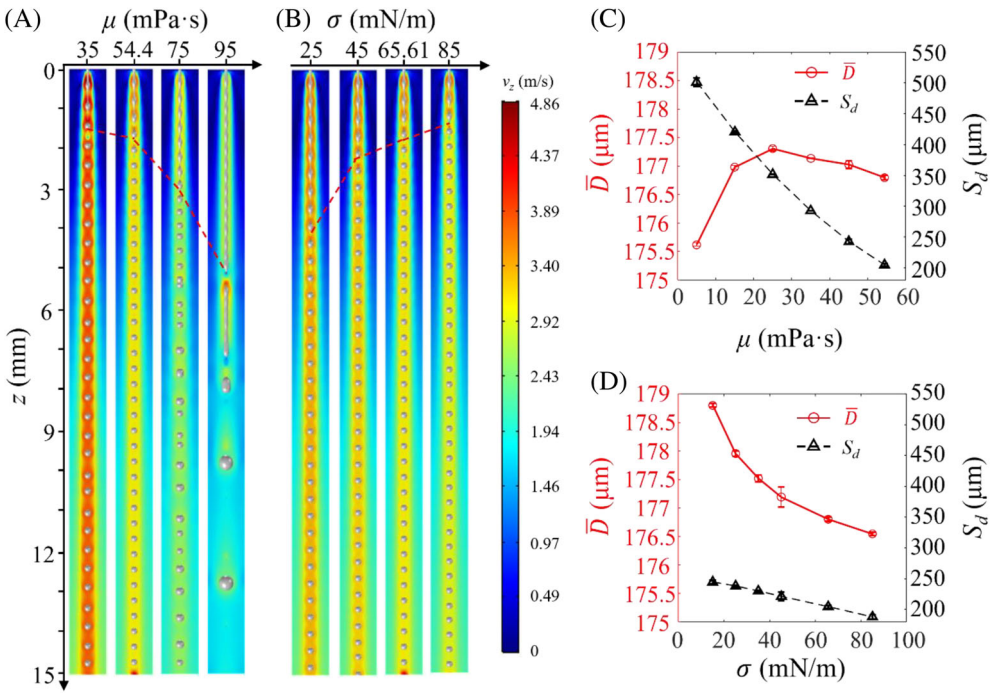

FIGURE 5 Results under different liquid properties that include (A), (C) viscosity and (B), (D) surface tension. (A) and (B) display droplet distributions at 10 ms, with red dashed lines marking the jet breakup positions; (C) and (D) are distributions of the average diameter of 50 droplets and average spacing between 50 neighboring droplets collected after 10 ms at the outlet of the out-nozzle model. Results are presented as mean ± SD.

quantitative understanding of droplet formation mechanisms. Consequently, a thorough analysis involving 253 cases has been conducted. Note that, a total of 266 cases were designed in this work, of which 6 explored the effect of surface tension and 7 for exploring the effect of nozzle radius under constant pressure. Surface tension has been excluded from hereinafter exploration due to its negligible effect on both droplet size and state transition of droplet distribution.

Consistent with our finding, frequency is also the key parameter in experiments to control the droplet distribution state.[23] The droplet distribution states under different combinations of frequency and four other parameters are summarized in Figure 6A–D. The results highlight four distinct droplet distribution states with different symbols. For monodispersed droplets (denoted by circles), droplet sizes are also illustrated with different colors.

Figure 6A shows four distinct droplet distribution patterns influenced by frequencies and inflow rates. At a fixed inflow rate, here take 1.3 g/min as an example. At low frequencies (<4 kHz), satellite droplets are produced along with the main droplets. When the frequency increases, droplets exhibit a monodisperse distribution (4–10 kHz). Further increasing the frequency results in droplet coalescence due to irregular jet breakup. Frequencies above 14 kHz lead to random jet breakup and disordered droplets. Similarly, for a fixed frequency, such as 8 kHz, the following phenomena can be observed. At lower inflow rates (<1.0 g/min), the liquid jet exhibits disordered breakup patterns. Increasing the inflow rate shifts the distribution state from disordered to coalescence, and then to a monodisperse distribution. Further increasing inflow rate, however, can give rise to droplets with satellites. Disordered droplet distribution tends to occur under low inflow rates and high frequencies, while satellite distribution tends to occur under high inflow rates and low frequencies. Monodispersed droplets and droplets with coalescence are observed between these two states. To maintain droplet uniformity, f and q_{in} should be varied synergistically—one has to be increased simultaneously with the other.

Regarding the factors of frequency and nozzle radius (Figure 6B), a different trend can be identified. With the increase of nozzle radius, the distribution states change from droplets with satellites to uniform to coalescence and eventually to disordered droplets. This variation is attributed to the negative correlation between the nozzle radius and jet velocity (under a constant inflow rate), which significantly influences the distribution modes. To produce monodisperse droplets under a higher frequency, a smaller nozzle is needed. The state transition pattern in the frequency and viscosity plot (Figure 6C) is similar to that in the frequency and nozzle radius plot (Figure 6B). A higher viscosity leads to a lower jet velocity, making it more likely to produce disordered droplets.

In contrast to the droplet distribution states influenced by frequency, inflow rate, nozzle radius, and viscosity, voltage appears to have little impact on jet breakup patterns at lower frequencies (<10 kHz, see Figure 6D). At higher frequencies, however, increasing voltage tends to shift the droplet distribution state from disordered to satellite patterns. It suggests that only at these relatively high frequencies, voltage can be adjusted to switch droplet distribution states.

Given the significant influence of frequency combined with three other factors (q_{in}, R_n, and μ) on the droplet distribution state, the Reynolds number ($Re = Du\rho/\mu = 2q_{in}/(\pi R_n \mu)$) is employed to combine the impact of the latter three. In this way, the droplet distribution states in Figure 6A–C can be incorporated into Figure 6E. Three zones can be identified in this plot. Two boundaries are plotted in Figure 6E to distinguish three distinct zones. Two piecewise functions were developed to quantitatively describe these boundaries.

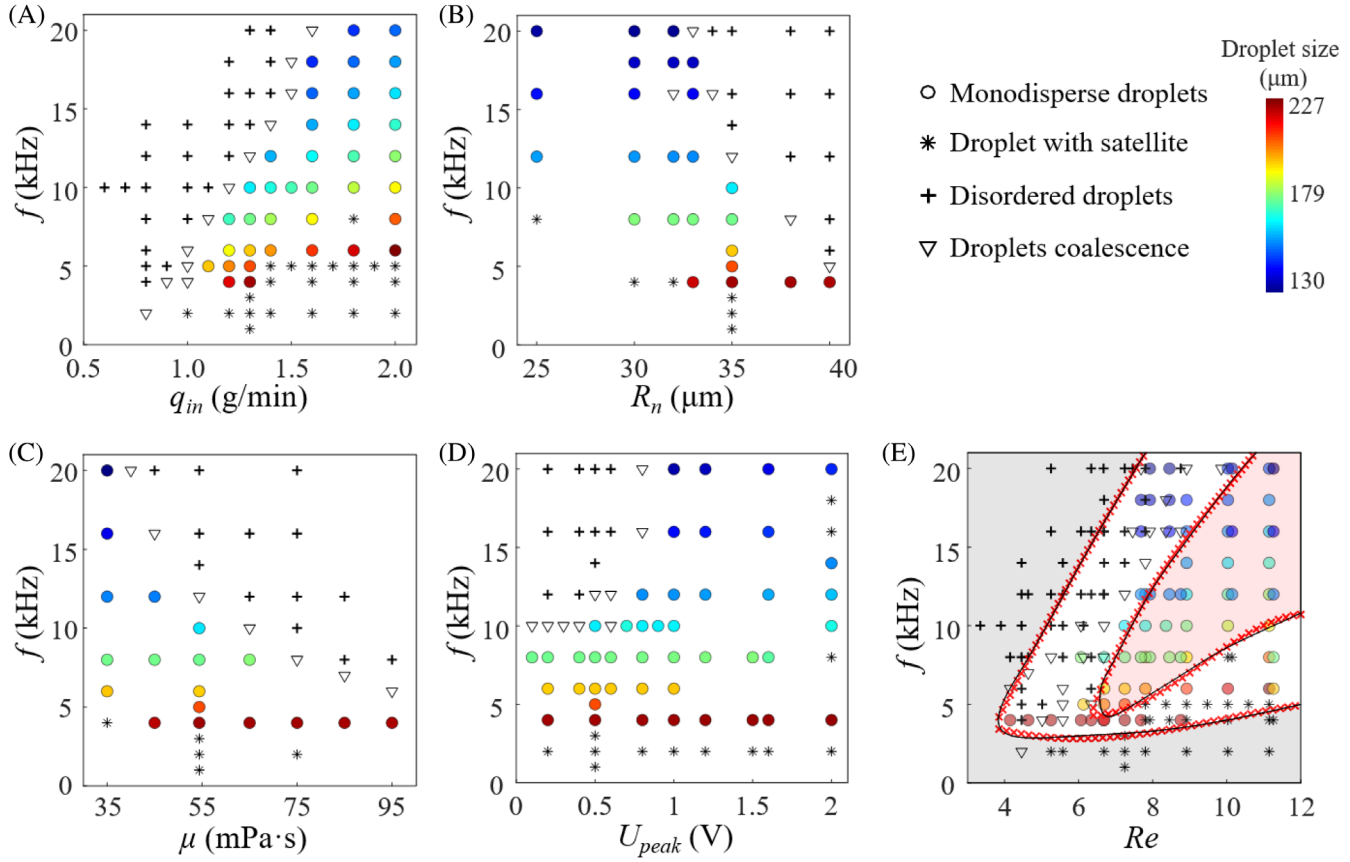

FIGURE 6 Droplet distribution states under different conditions: Different combinations of frequency and (A) inflow rate, (B) nozzle radius, (C) liquid viscosity, (D) peak voltage, and (E) Reynolds number. In (E), three zones are highlighted: (1) the uniform zone, that is, the shaded area with pink color, indicating conditions that can offer monodisperse droplets, (2) the nonuniform zone, that is, the shaded area with gray color, indicating nonuniform droplet generation, and (3) the transition zone, where all four distribution states are possible. The red "x" symbols represent the fitting formulas for the two boundaries.

For the boundary between the uniform zone and the transition zone:

$$f=\begin{cases}0.08296Re^3-2.477Re^2+27.51Re-91.58, & \text{the upper part}\\ -0.06515Re^3+1.819Re^2-15.27Re+44.6, & \text{the lower part}\end{cases}. \tag{12}$$

For the boundary between the transition zone and the nonuniform zone:

$$f=\begin{cases}-0.112Re^2+5.555Re-15.53, & \text{the upper part}\\ -0.00944Re^3+0.2841Re^2-2.38Re+8.921, & \text{the lower part}\end{cases} \tag{13}$$

where f is the frequency in kHz.

The shaded area with pink color is the uniform zone, which offers desirable conditions for monodisperse droplet generation. The shaded area with gray color is the nonuniform zone, indicating conditions that should be avoided since under which, there is no chance to get monodisperse droplets. The area in between is the transition zone, where four distribution states coexist. It is found that, within the range of parameter values under investigation, stable production of monodisperse droplets requires a larger Re at a higher frequency. If non-uniform droplets are generated, jet breakup mode can be tuned to shift the distribution states. For instance, if the breakup mode is disordered, reducing the frequency or increasing Re is a feasible method to pursue mono-dispersity. Operating the nozzle under conditions in the uniform zone can greatly facilitate monodisperse droplet generation.

We now address the issue of droplet size control. It can be concluded from Figure 6A–D that the size of the monodisperse droplets is mainly regulated by f and q_{in}. Larger droplets can be obtained by reducing f or increasing q_{in}. For the piezoelectric ceramic nozzle, the following relationship can be obtained based on mass conservation:

$$\frac{4}{3}\pi\left(\frac{\hat{D}}{2}\right)^3\rho_l=\frac{q_{in}}{f}, \tag{14}$$

Thus, the derived average diameter of uniform-sized droplets is:

$$\hat{D}=\sqrt[3]{\frac{6q_{in}}{\pi\rho_l f}}. \tag{15}$$

By comparison, the error between the calculated droplet size and the simulated result of most cases is less than 5%, demonstrating the

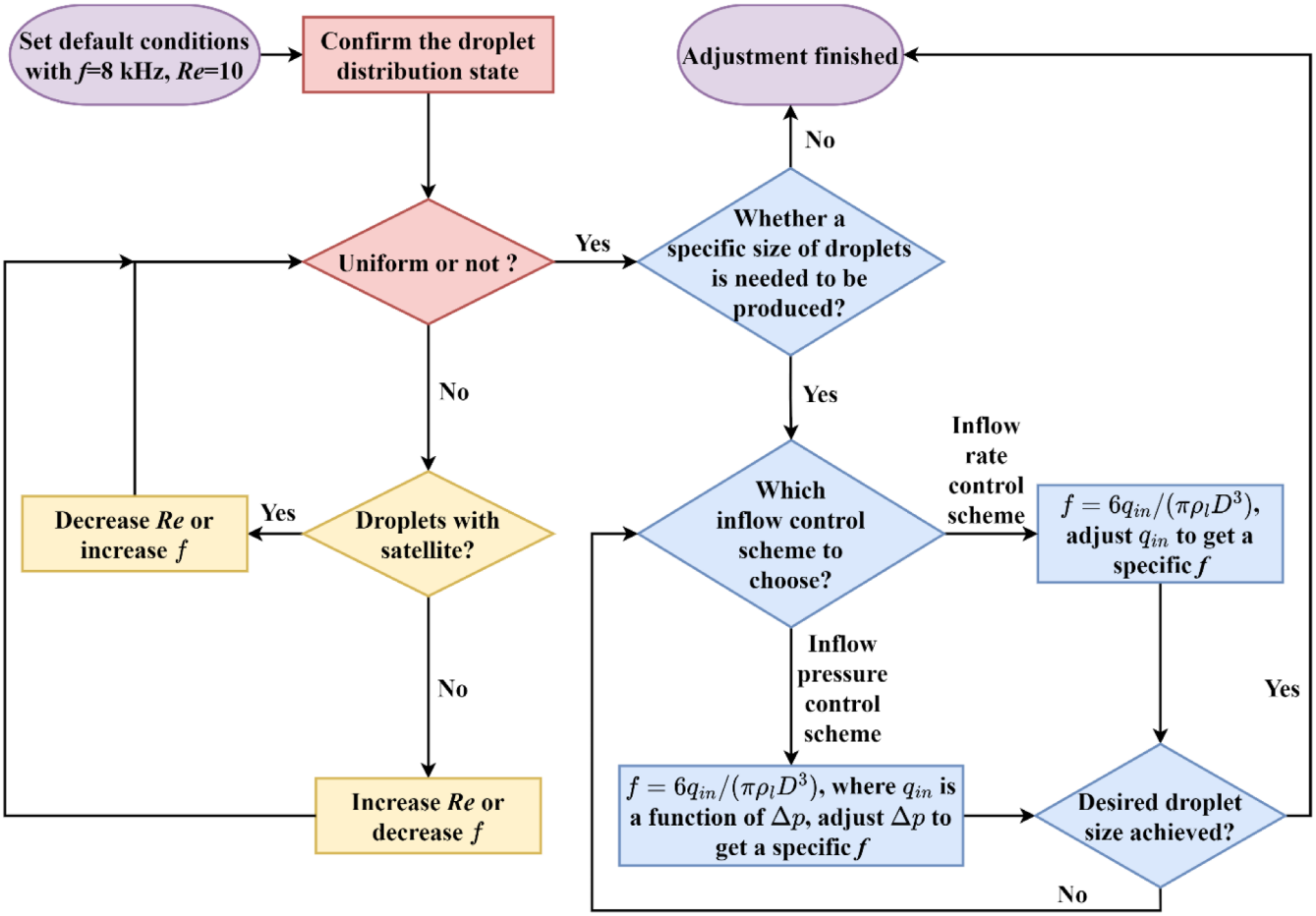

FIGURE 7 Procedures to generate uniform droplets with a specified size for a certain liquid by using piezoelectric pulsation-driven glass nozzles. An increase of *Re* means either (1) under inflow rate control scheme: An increase of q_{in}, or decrease of R_n; or (2) under inflow pressure control scheme: An increase of p_{in}, or increase of R_n (to increase q_{in}).

reliability of the formula in predicting the droplet size. Furthermore, Equation (15) shows that the droplet size changes only with inflow rate q_{in}, density ρ_l and disturbance frequency f and is unaffected by other parameters including R_n (Figure 6B), μ (Figure 6C) and U_{peak} (Figure 6D). According to the Bernoulli's equation, the fluid between inlet and outlet surfaces of the atomizer should follow

$$g\Delta z + \frac{\Delta p}{\rho} + \Delta\frac{u^2}{2} = h_f, \tag{16}$$

where Δz (m) is the distance between inlet and outlet surfaces, Δp (Pa) is the pressure difference and $h_f = 32\mu lu/d^2$ is the laminar flow resistance in a straight tube. Then the velocity at specific cross section can be derived, and flow rate could be expressed as:

$$q_{in} = f(\Delta p, R_n, \mu, \rho_l) \tag{17}$$

which is a function of pressure difference, nozzle radius, and liquid properties. It indicates that the nozzle radius R_n is one of the factors influencing the inflow rate, which is crucial for adjusting droplet size. The detailed derivation and the final equation form are given in Supplementary Material S7. According to Equation (17), adjusting pressure is another way to control the inflow rate. Two control schemes can be adopted for the inflow fluid: (1) inflow rate control scheme, and (2) inflow pressure control scheme. Most previous experimental efforts used the second scheme where pressure is manipulated directly. Since the pressure is a function of inflow rate and nozzle radius, Wu et al.[31] realized control of the droplet size by adjusting the nozzle radius.

For a specific liquid, the relationship between the inflow rate, pressure difference, and nozzle radius can be derived (see Supplementary Material S7). To obtain droplets of a specified size for a specific liquid, one can adjust f together with either (1) q_{in}, or (2) p_{in} and R_n. With the parameter values identified in this work, droplet diameters between 128 and 227 μm could be achieved, corresponding to 1.83–3.24 times the nozzle diameter.

To facilitate on-aim size control of monodispersed droplets with certain rheological properties, a guideline has been developed to offer a straightforward operational procedure (Figure 7). Based on the provided default settings, the steps outlined in Figure 7 can be easily followed. If the droplet distribution is uniform, adjustments can be made to the corresponding parameters based on the desired droplet size. If

the droplets exhibit non-uniformity, some parameters can be iteratively adjusted until reaching a uniform distribution. This process is expected to greatly accelerate the production of monodispersed droplets of a specific size.

4 | CONCLUSION

In this work, a new multi-physics model has been developed to realize the simulation of the complete atomization process by piezoelectric pulsation-driven glass nozzles, aiming at addressing the challenge of producing monodisperse droplets of a specified size. Different from reported models, a semi-empirical relationship was developed, enabling the simulation of the complete atomization process including phenomena in and outside of the nozzle without the need of time-consuming in-nozzle CFD model.

This work has discussed the jet breakup and four states of droplet distribution, including disordered droplets, droplets with coalescence, monodisperse droplets, and droplets with satellites. To identify the conditions for producing monodisperse droplets, different parameters have been examined, including frequency, voltage, inflow rate, nozzle size, liquid viscosity, and surface tension. The results reveal that one of the three following methods can lead to a transition from disordered to coalescence to monodisperse droplet distribution and then to satellite formation: (1) decreasing the frequency, (2) increasing *Re* (by either increasing the inflow rate, or decreasing the nozzle radius (under inflow rate control scheme), or increasing the nozzle radius (under inflow pressure control scheme), or increasing inflow pressure or decreasing liquid viscosity), and (3) increasing the voltage. Surface tension primarily affects the liquid jet length, and has a negligible impact on droplet distribution states. This phenomenon is closely linked to the liquid jet velocity resulting from differences in operating conditions or liquid properties. When the axial velocity of liquid jet is low, the jet lacks sufficient inertial force to break into droplets. As the axial velocity increases, the inertial force balances with the surface tension and viscous force, resulting in more uniform droplets. Further velocity increases lead to greater spacings between perturbations, causing the thread to break further into small independent satellite droplets.

The droplet size can be estimated by $\widehat{D} = \sqrt[3]{\frac{6q_{in}}{\pi\rho_l f}}$, while the inflow can be controlled by either manipulating inflow rate or inflow pressure. Droplet size is influenced by nozzle radius only for the constant pressure control scheme. Furthermore, droplets of specified sizes can be produced by adjusting the material and operating parameters. An operational procedure has been developed to facilitate on-aim-sized monodisperse droplet generation.

This work enhances our understanding of the piezoelectric pulsation-driven atomization process and offers an effective guideline for generating droplets of specified sizes. The computationally efficient model developed here can save enormous trial-and-error experimental costs in identifying optimal conditions for uniform droplet generation.

AUTHOR CONTRIBUTIONS

Jinping Zha: Investigation; writing – original draft; methodology; software; validation; visualization; formal analysis; data curation. **Hong Zhu:** Formal analysis; writing – review and editing. **Liangchao Shang:** Investigation; methodology; software. **Yongchen Lu:** Writing – review and editing; formal analysis. **Winston Duo Wu:** Writing – review and editing; conceptualization; resources. **Xiao Dong Chen:** Conceptualization; writing – review and editing; resources. **Jie Xiao:** Conceptualization; investigation; funding acquisition; writing – review and editing; methodology; formal analysis; project administration; supervision; resources; visualization.

ACKNOWLEDGMENTS

We are grateful for the financial support from the National Natural Science Foundation of China (21978184, 22278284), the "Jiangsu Innovation and Entrepreneurship (Shuang Chuang) Program", the "Jiangsu Specially Appointed Professors Program", and the "Priority Academic Program Development (PAPD) of Jiangsu Higher Education Institutions".

DATA AVAILABILITY STATEMENT

The governing Equations (S1), initial and boundary conditions (S2), time step independence study (S3), the effect of different PZT geometries and locations (S4), the reliability of the semi-empirical relationship (S5), the validity of the assumption of fully developed flow (S6), and derivation of the relationship between the inflow rate, pressure difference and the nozzle radius (S7) are listed in the Supplementary Materials. The size data of monodispersed droplets in Figures 3–6 are tabulated in the Supplementary Data File (a zip file).

ORCID

Jie Xiao https://orcid.org/0000-0001-7842-7862

REFERENCES

1. Yoshimura K, Kishimoto M, Suemune T. Inkjet printing technology. *OKI Tech Rev*. 1998;64:61-64.
2. Sontti SG, Atta A. Numerical insights on controlled droplet formation in a microfluidic flow-focusing device. *Ind Eng Chem Res*. 2020;59(9):3702-3716.
3. Kalantarifard A, Alizadeh-Haghighi E, Saateh A, Elbuken C. Theoretical and experimental limits of monodisperse droplet generation. *Chem Eng Sci*. 2021;229:116093.
4. Gavini E, Manunta L, Giua S, Achenza G, Giunchedi P. Spray-dried poly(D,L-Lactide) microspheres containing carboplatin for veterinary use: in vitro and in vivo studies. *AAPS PharmSciTech*. 2005;6(1):E108-E114.
5. Pavia D. Efficacy and safety of inhalation therapy in chronic obstructive pulmonary disease and asthma. *Respirology*. 1997;2:S5-S10.
6. Plateau J. Experimental and theoretical steady state of liquids subjected to nothing but molecular forces. *Soft Matter*. 1873;17(14):3975.
7. Rayleigh L. On the instability of jets. *Proc London Math Soc*. 1878;11:4-13.
8. O'Sullivan JJ, Norwood EA, O'Mahony JA, Kelly AL. Atomisation technologies used in spray drying in the dairy industry: a review. *J Food Eng*. 2019;243:57-69.
9. Schroder T, Walzel P. Design of laminar operating rotary atomizers under consideration of the detachment geometry. *Chem Eng Technol*. 1998;21(4):349-354.

10. Xu S, Nie Z, Seo M, et al. Generation of monodisperse particles by using microfluidics: control over size, shape, and composition. *Angew Chem Int Ed*. 2005;44(5):724-728.
11. Lu Y, Liu X, Liu X, Chen Y. Robust generation of monodisperse droplets using a microfluidic step emulsification device with triangular nozzle. *AIChE J*. 2023;69(11):e18202.
12. Yan Z, Huang H, Pan Z. Bubble breakup and boiling heat transfer in Y-shaped bifurcating microchannels. *AIChE J*. 2022;69(2):e17836.
13. Sheng L, Chang Y, Wang J, Deng J, Luo G. Remarkable improvement of gas–liquid mass transfer by modifying the structure of conventional T-junction microchannel. *AIChE J*. 2023;69(7):e18089.
14. Zhang J, Ling SD, Chen A, Chen Z, Ma W, Xu J. The liquid–liquid flow dynamics and droplet formation in a modified step T-junction microchannel. *AIChE J*. 2022;68(6):e17611.
15. Zhang C, Yu C, Liu X, Jin O, Chen Y. Steady deformation characteristics of double emulsion droplet in shear flow. *Acta Phys Sin*. 2016;65(20):204704.
16. Liu X, Hao G, Li B, Chen Y. Experimental study on the electrohydrodynamic deformation of droplets in a combined DC electric field and shear flow field. *Fundam Res*. 2023;3(2):274-287.
17. Meesters GMH, Vercoulen PHW, Marijnissen JCM, Scarlett B. Generation of micron-sized droplets from the Taylor cone. *J Aerosol Sci*. 1992;23(1):37-49.
18. Liou TM, Chan CY, Shih KC. Effects of actuating waveform, ink property, and nozzle size on piezoelectrically driven inkjet droplets. *Microfluid Nanofluid*. 2010;8(5):575-586.
19. Ozen O, Aubry N, Papageorgiou DT, Petropoulos PG. Monodisperse drop formation in square microchannels. *Phys Rev Lett*. 2006;96(14):144501.
20. Liu H, Wang Z, Gao L, et al. Optofluidic resonance of a transparent liquid jet excited by a continuous wave laser. *Phys Rev Lett*. 2021;127(24):244502.
21. Duan H, Romay FJ, Li C, Naqwi A, Deng W, Liu BYH. Generation of monodisperse aerosols by combining aerodynamic flow-focusing and mechanical perturbation. *Aerosol Sci Tech*. 2015;50(1):17-25.
22. Vassallo P, Ashgriz N. Satellite formation and merging in liquid jet breakup. *Proc R Soc London, Ser A*. 1991;433(1888):269-286.
23. Wu WD, Lin SX, Chen XD. Monodisperse droplet formation through a continuous jet break-up using glass nozzles operated with piezoelectric pulsation. *AIChE J*. 2011;57(6):1386-1392.
24. Wu WD, Amelia R, Hao N, et al. Assembly of uniform photoluminescent microcomposites using a novel micro-fluidic-jet-spray-dryer. *AIChE J*. 2011;57(10):2726-2737.
25. Jiang T, Yan S, Zhang S, Yin Q, Chen XD, Wu WD. Uniform lactose microspheres with high crystallinity fabricated by micro-fluidic spray drying technology combined with post-treatment process. *Powder Technol*. 2021;392:690-702.
26. Mu K, Si T, Li E, Xu RX, Ding H. Numerical study on droplet generation in axisymmetric flow focusing upon actuation. *Phys Fluids*. 2018;30(1):012111.
27. Xiao Y, Zhang W, Wang P, Li H. Numerical simulation and experimental research of micro-droplet generation by directly actuated piezoelectric nozzle. *J Mech Eng*. 2020;56(17):233-239.
28. Wei H, Xiao X, Yin Z, Yi M, Zou H. A waveform design method for high DPI piezoelectric inkjet print-head based on numerical simulation. *Microsyst Technol*. 2017;23(12):5365-5373.
29. Zha J, Shang L, Wu WD, Chen XD, Xiao J. A velocity coupling method for atomization modeling: application to piezoelectric pulsation-driven glass nozzles. *Ind Eng Chem Res*. 2024;63(39):16915-16927.
30. Scharfman BE, Techet AH, Bush JWM, Bourouiba L. Visualization of sneeze ejecta: steps of fluid fragmentation leading to respiratory droplets. *Exp Fluids*. 2016;57(2):24.
31. Wu WD, Patel KC, Rogers S, Chen XD. Monodisperse droplet generators as potential atomizers for spray drying technology. *Drying Technol*. 2007;25(12):1907-1916.
32. Chen Y, Huang Y, Kuo C, Chang S. Investigation of design parameters for droplet generators driven by piezoelectric actuators. *Int J Mech Sci*. 2007;49(6):733-740.

SUPPORTING INFORMATION

Additional supporting information can be found online in the Supporting Information section at the end of this article.

How to cite this article: Zha J, Zhu H, Shang L, et al. On-aim generation of monodisperse droplets from piezoelectric pulsation-driven glass nozzles. *AIChE J*. 2025;e18744. doi:10.1002/aic.18744